Optics Letters

Bound valley edge states in the continuum

Yadian Feng,[1] Zhanyuan Zhang,[1,5] Feifei Qin,[1] Zhihao Lan,[2,6] Wei E. I. Sha,[3] and Yi Xu[4]

[1]Department of Electronic Engineering, College of Information Science and Technology, Jinan University, Guangzhou, 510632, China
[2]Department of Electronic and Electrical Engineering, University College London, Torrington Place, London, WC1E 7JE, United Kingdom
[3]State Key Laboratory of Modern Optical Instrumentation, College of Information Science and Electronic Engineering, Zhejiang University, Hangzhou 310027, China
[4]Institute of Advanced Photonics Technology, School of Information Engineering, Guangdong University of Technology, Guangzhou, 510006, China
[5]e-mail: zzyzhanyuan@gmail.com
[6]e-mail: z.lan@ucl.ac.uk

Received 9 May 2022; revised 30 May 2022; accepted 30 May 2022; posted 31 May 2022; published 14 June 2022

Topological valley photonics provides a unique way to manipulate the flow of light. In general, valley edge states that exhibit unidirectional propagation and are immune to defects and disorders could be realized at the interface between two valley photonic crystals with opposite valley Chern numbers. Herein, by merging the physics of valley edge states and bound states in the continuum, we propose and numerically demonstrate a novel, to the best of our knowledge, concept of edge states termed bound valley edge states in the continuum, which enjoys the topological features of valley edge states, such as, unidirectional propagation and immunity to disorders, but are formed at the interface between air and a single valley photonic crystal. Our results not only provide an effective way to reduce the size of valley photonic structures but also facilitate new applications where the proposed concept of bound valley edge states in the continuum could be exploited for optical sensing and unidirectional waveguiding.

https://doi.org/10.1364/OL.463458

Several family members of quantum-Hall-related topological electronic states in condensed matter physics have found their counterparts in photonic systems, such as, electromagnetic analogs of quantum Hall edge states in real or synthetic magnetic fields [1–5], Z_2 photonic quantum spin Hall insulators [6–13], and photonic quantum valley Hall insulators [14–24]. Among them, the photonic valley Hall structures characterized by valley degrees of freedom require no magnetic effects or intricate constructions of photonic pseudospins, but only need inversion symmetry breaking, thus could be more easily fabricated using all-dielectric materials compatible with modern micro–nano fabrication technology for compact on-chip optical devices [25,26].

The valley refers to a local minimum/maximum in the conduction/valence band, which in general emerges at high-symmetry points of the Brillouin zone, e.g., the K/K′ point in hexagonal lattices with broken inversion symmetry [25,26]. Due to the nontrivial local distributions of the Berry curvature around K/K′ (with opposite signs at K and K′), one could define a valley Chern number by integrating the Berry curvature around K/K′. According to the bulk-edge correspondence principle [27], topological valley edge states can be constructed along a domain wall between two PhCs with opposite valley Chern numbers. Photonic valley Hall edge states not only exhibit interesting features, such as, robust unidirectional transport of light through sharp corners which could be effectively manipulated by choosing chirality of the excitation source, but also offer a broad range of potential applications, e.g., on-chip communications [28–31], reconfigurable devices [32,33], valley-Hall topological lasers [34], chiral topological photonics coupled with quantum emitters [35,36], second-harmonic generation [37], and slow-light waveguides [38,39].

In order to further facilitate the on-chip applications of topological photonics, it is necessary to minimize the size of the photonic structures. Photonic modes could be localized on the surface of PhCs due to the mechanism of BIC [40,41], which provides an effective way to confine light in the radiation continuum without further cladding layers. BIC has enabled unprecedented explorations of interesting physics, such as the topological properties of polarization singularities [42,43] and their evolutions in momentum space [44–47], and facilitated many promising applications ranging from high-performance sensing [48] to lasing [49]. By merging the physics of topological edge states with the BIC, bound topological edge states in the continuum with the prominent feature of pseudospin-momentum locking unidirectional propagation were studied recently where the helical edge states of photonic quantum spin Hall insulators were localized on the surface of a single topological nontrivial PhC [50]. Considering this result, it is natural and interesting to ask whether other members of the quantum-Hall-related topological edge states, such as quantum valley Hall edge states, could also be confined to the surface of a single valley PhC by the physics of BIC.

In this Letter, we demonstrate that merging the physics of BIC with photonic valley Hall edge states leads to a new type of edge states, which we term bound valley edge states in the continuum living on the surface of a single all-dielectric valley PhC. These novel states will not only open a new avenue for manipulating light transport within radiation continuum, but could also be

used to minimize the size of topological photonic structures for more compact integrated photonics devices.

We consider a two-dimensional honeycomb-like all-dielectric valley PhC to demonstrate the idea of bound valley edge states in the continuum. The unit cell of the valley PhC is shown in Fig. 1(a), which consists of two types of cylinders ($\epsilon_r = 9.6$) with radii r_a and r_b. The band structure for the transverse magnetic (TM) modes (E_z polarized) of the valley PhC when $r_a = r_b = 0.226a$ is shown in Fig. 1(b), from which one can see that a Dirac point (marked by a red dot) is formed between the fourth and fifth bands at the K/K′ point with normalized frequency $a/\lambda \simeq 0.58$. Note that we focus on this Dirac point rather than the one between the first and second bands at lower frequency because this Dirac point lies outside the light cone which can be intuitively seen from Fig. 2(a), which allows us to explore the effect of radiation continuum on the valley edge states. The inversion symmetry of the PhC could be broken by setting $r_a \neq r_b$, which will gap out the Dirac point, giving rise to a valley gap [25,26]. The corresponding band structure of the PhC at $r_a = 0.258a$ and $r_b = 0.194a$ is shown in Fig. 1(c), where the resulting valley gap is marked by a red box. The phase distributions of the eigenmodes (E_z) at K and K′ points for the fourth and fifth bands below and above the valley gap are shown in Fig. 1(d), from which one can see that the phases of the K and K′ valley states around the center of the unit cell increase clockwise/counterclockwise by 2π. To study the topological edge states of the valley PhC mediated by BIC, we consider a semi-infinite PhC whose supercell is given in Fig. 1(e), where Bloch periodic boundary conditions and perfect matching layer (PML) used in the numerical calculations are also marked. Note to tune the properties of the bound valley edge states in the continuum, we modify the size r_d of the boundary cylinders.

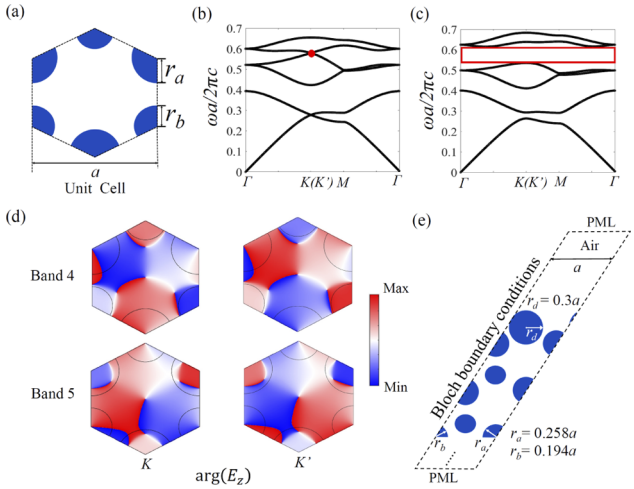

Fig. 1. (a) Schematic of the unit cell of the valley photonic crystals (PhC), which consists of two types of dielectric cylinders ($\epsilon_r = 9.6$) with radii r_a and r_b. The lattice constant is $a = 31$ mm, and the background material is air ($\epsilon_r = 1$). (b) The band structure of the valley PhC when $r_a = r_b = 0.226a$, in which the Dirac point we mention, is marked by a red dot. (c) The band structure at $r_a = 0.258a$ and $r_b = 0.194a$, where the Dirac point is gapped out, resulting in a valley gap denoted by a red box. (d) Phase distributions of E_z at K and K′ for the fourth and fifth bands below and above the bandgap shown in panel (c). (e) The supercell of the topological valley PhC supporting bound states in the continuum (BICs), where the valley PhC is truncated by boundary sites with radius $r_d = 0.3a$.

Figure 2(a) shows the projected band structure of the truncated valley PhC in Fig. 1(e) calculated using the finite element method (FEM). The black dashed box denotes the frequency range where the bound valley edge states in the continuum appear, which is enlarged and shown in Fig. 2(b). As can be seen from Fig. 2(b),

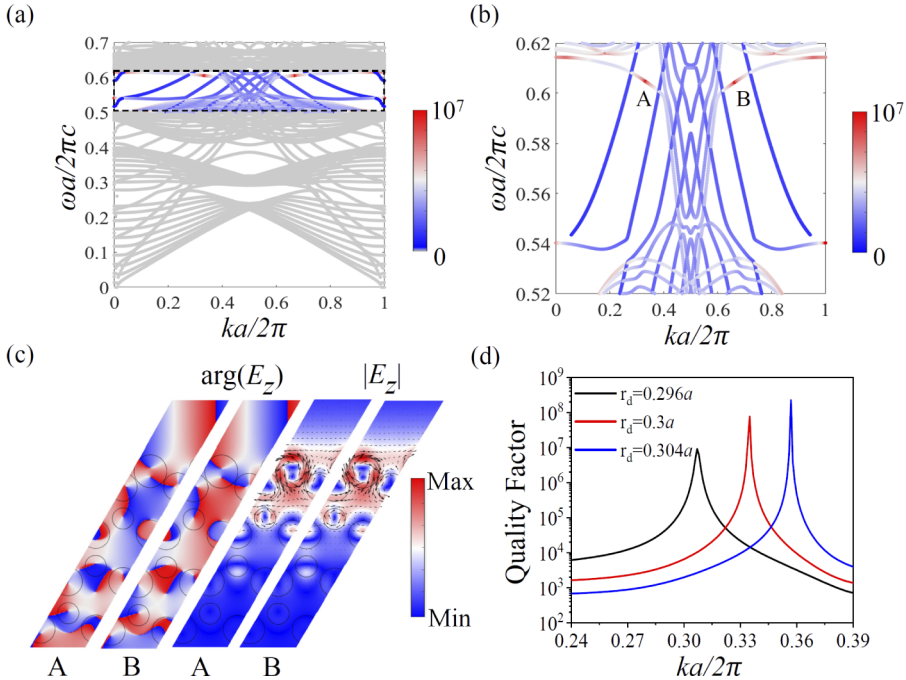

Fig. 2. (a) Projected band structure of the valley PhC shown in Fig. 1(e) at $r_d = 0.3a$, where the mentioned frequency range is marked by a black dashed box, and the corresponding Q factors of the eigenmodes are given by the color code. (b) Zoomed-in view of the region inside the black dashed box of panel (a), where two emergent BICs are indicated by A and B. (c) Phase and amplitude distributions of E_z for the two BICs indicated by A and B in panel (b). Poynting vectors are denoted by black arrows. (d) Q factors of the band in which the BIC locates for three different radii of the boundary sites.

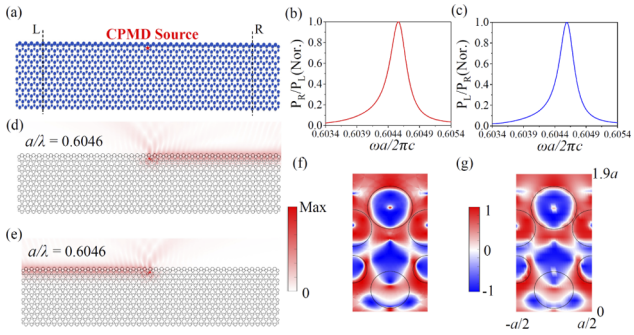

Fig. 3. (a) A finite PhC structure of 45 periods supporting quasi-bound valley edge states in the continuum, where the location of circularly polarized magnetic dipole (CPMD) source is marked by the red star. (b), (c) The normalized transmission efficiency P_R/P_L and P_L/P_R under the excitation of CPMD source at two opposite spin states as a function of the excitation frequency. Here P_R and P_L are evaluated by integrating the power along the dashed lines L and R marked in panel (a). (d), (e) Distributions of the electric field amplitude ($|E_z|$) at the resonant transmission peaks in panels (b) and (c). (f) Stokes parameter S_3 retrieved from the eigenmode A of Fig. 2(b). (g) Directionality D(x,y) retrieved from the transmission results by scanning the position of a pseudospin-up magnetic dipole excitation source.

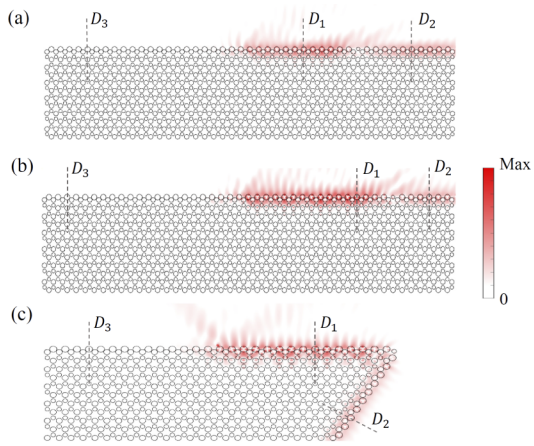

Fig. 4. Robustness of the quasi-bound valley edge states in the continuum under the influence of (a), (b) a smaller defect cylinder at different locations along the propagation path, and (c) a 60° waveguide bend.

a pair of high quality (Q) factor eigenmodes (indicated by A and B) with k = $0.335(2\pi/a)$ and k = $0.665(2\pi/a)$ above the light cone exists within the valley gap, where the Q factors are calculated from $Q = -\mathrm{Re}(\omega)/2\mathrm{Im}(\omega)$. Figure 2(c) shows the phase and amplitude distributions of E_z for this pair of states. A second-order phase vortex center can be clearly identified within the boundary sites and the electric field is also perfectly localized around the truncated edge without any leakage to the air. At the same time, Poynting vectors are superimposed on the amplitude distribution of E_z by black arrows, which rotate counterclockwise or clockwise around the center of the phase vortex for mode A or B, respectively. The distributions of Poynting vectors indicate a tendency that the electromagnetic energy flows from one supercell to its adjacent supercell, forming an effective waveguiding channel. The momentum of the bound valley edge state in the continuum can be effectively tuned by changing the radius r_d of boundary cylinders as demonstrated in Fig. 2(d). The closer the bound valley edge state is to the K(K′) valley, the better the topological properties of this state are. In the following, we focus on the bound valley states in the continuum at $r_d = 0.3a$.

To study the propagation behaviors of the bound valley edge states, we consider a finite valley PhC with 45 periods under the excitation of CPMD sources [indicated by the red star in Fig. 3(a)] with two opposite spin states. The left (right) propagating energy flux P_L (P_R) is calculated at the dashed line L(R) marked in Fig. 3(a), and their ratio is plotted as a function of the excitation frequency to evaluate the coupling between the CPMD source and the quasi-bound valley edge states in the continuum. The corresponding normalized results P_R/P_L and P_L/P_R are shown in Fig. 3(b) and 3(c) for the pseudospin-down and pseudospin-up sources, respectively, from which one can see that unidirectional edge states of the same frequency propagating along the opposite directions are excited by CPMD sources with opposite pseudospin states. Distributions of the electric field amplitude ($|E_z|$) at the peaks of Fig. 3(b) and 3(c) are shown in Fig. 3(d) and 3(e), respectively, where unidirectional propagations can be observed with the electric field confined near the boundary sites. The leakage to the air is because of the weak coupling between the CPMD sources and the structure. To show that the propagation direction of the bound valley edge states in the continuum could be further manipulated by changing the location of the CPMD source, we calculate $D(x,y) = 2\mathrm{Im}(H_x^* H_y)/(|H_x|^2 + |H_y|^2)$ that is similar to the Stokes parameter S_3 for guided modes [51] at the frequency of the bound valley edge state for eigenmode A, as shown in Fig. 3(f). The corresponding excitation results of the directionality $D(x,y) = (P_R - P_L)/(P_R + P_L)$ obtained by scanning the position of the CPMD source at the same frequency are shown in Fig. 3(g). Both results agree reasonably well with each other, indicating that the excitation direction of bound valley edge state in the continuum can be effectively controlled by tuning the location of the CPMD source.

In order to verify the topological robustness of these novel bound states, we consider their transmissions when a defect site ($r_s = 0.196a$) is introduced along the propagation path. From the distribution of electric field amplitude ($|E_z|$) with the defect shown in Fig. 4(a) under a pseudospin-down CPMD excitation source, the unidirectional propagating wave can successfully bypass the defect without being backscattered, where the resulting electric field is still well confined near the boundary of the PhC. The power flux integration at the three dashed lines marked in Fig. 4(a) is used to quantitatively evaluate the degree of defect immunity of this bound valley edge state in the continuum. The transmission efficiency (D_2/D_1) reaches 65.5 % and the normalized directionality [$(D_2 - D_3)/(D_2 + D_3)$] reaches 87.8 %, which verifies that this structure has a good immunity against defect compared with the conventional surface valley edge state [52]. In order to show the generality of this effect, in Fig. 4(b) the defect (r_s=0.192a) is randomly introduced at another location, and the result under the same excitation condition is shown in Fig. 4(b), from which one can see that the unidirectional edge state can still bypass the defect. The corresponding transmission efficiency (D_2/D_1) reaches 63.5 % and the normalized directionality [$(D_2 - D_3)/(D_2 + D_3)$] reaches 96.8 %.

Finally, we consider the propagation of these bound states against a sharp bend (60°). Under the excitation of the

pseudospin-up CPMD source, the distribution of the electric field amplitude ($|E_z|$) shown in Fig. 4(c) demonstrates that the unidirectional bound state can propagate through the sharp corner of this finite PhC, where the transmission efficiency (D_2/D_1) reaches 66.4 % and normalized directionality [$(D_2 - D_3)/(D_2 + D_3)$] reaches 99.6 %. These results validate the good topological robustness of the proposed bound valley edge states in the continuum. It should be noted that due to momentum mismatch, though some of the energy is scattered at the defect and the bend, most of the energy can be transmitted. This is because the BIC nature of these edge states can only suppress the scattering at a specific momentum k, which could make this kind of bound topological edge states in the continuum suitable for sensing.

In conclusion, we have proposed and numerically demonstrated a valley PhC supporting BICs. Such bound valley edge states in the continuum could be effectively tuned by the size of boundary sites and their unidirectional propagation was demonstrated to be robust against defects and sharp corners. We believe these novel bound states based on a single valley PhC might have broad prospects in the field of integrated photonic devices. The proposed mechanism could also be applied to other wave systems. It is anticipated that our findings would broaden the scope of topological valley photonics and enrich the research implications of both topological photonics and BICs.

Funding. Key Technologies Research and Development Program (2018YFB1801001); Guangdong Introducing Innovative and Entrepreneurial Teams of "The Pearl River Talent Recruitment Program" (2019ZT08X340); National Natural Science Foundation of China (91750110).

Disclosures. The authors declare no conflicts of interest.

Data availability. Data underlying the results presented in this paper are not publicly available at this time but may be obtained from the authors upon reasonable request.

REFERENCES

1. F. D. M. Haldane and S. Raghu, Phys. Rev. Lett. **100**, 013904 (2008).
2. Z. Wang, Y. Chong, J. D. Joannopoulos, and M. Soljacić, Nature **461**, 772 (2009).
3. Y. Poo, R. Wu, Z. Lin, Y. Yang, and C. Chan, Phys. Rev. Lett. **106**, 093903 (2011).
4. M. Hafezi, E. A. Demler, M. D. Lukin, and J. M. Taylor, Nat. Phys. **7**, 907 (2011).
5. K. Fang, Z. Yu, and S. Fan, Nat. Photonics **6**, 782 (2012).
6. A. B. Khanikaev, S. H. Mousavi, W.-K. Tse, M. Kargarian, A. H. MacDonald, and G. Shvets, Nat. Mater. **12**, 233 (2013).
7. W. J. Chen, S. J. Jiang, X. D. Chen, B. Zhu, L. Zhou, J. W. Dong, and C. T. Chan, Nat. Commun. **5**, 5782 (2014).
8. T. Ma, A. B. Khanikaev, S. H. Mousavi, and G. Shvets, Phys. Rev. Lett. **114**, 127401 (2015).
9. L. H. Wu and X. Hu, Phys. Rev. Lett. **114**, 223901 (2015).
10. C. He, X. C. Sun, X. P. Liu, M. H. Lu, Y. Chen, L. Feng, and Y. F. Chen, Proc. Natl. Acad. Sci. U. S. A. **113**, 4924 (2016).
11. F. Gao, Z. Gao, X. Shi, Z. Yang, X. Lin, H. Xu, J. D. Joannopoulos, M. Soljačić, H. Chen, L. Lu, Y. Chong, and B. Zhang, Nat. Commun. **7**, 11619 (2016).
12. X. D. Chen, W. M. Deng, F. L. Zhao, and J. W. Dong, Laser Photonics Rev. **12**, 1800073 (2018).
13. Y. Wei, B. Yan, Y. Peng, A. Shi, D. Zhao, R. Peng, Y. Xiang, and J. Liu, Opt. Lett. **46**, 3941 (2021).
14. T. Ma and G. Shvets, New J. Phys. **18**, 025012 (2016).
15. J. W. Dong, X. D. Chen, H. Zhu, Y. Wang, and X. Zhang, Nat. Mater. **16**, 298 (2017).
16. X. D. Chen, F. L. Zhao, M. Chen, and J. W. Dong, Phys. Rev. B **96**, 020202 (2017).
17. Y. Yang, H. Jiang, and Z. H. Hang, Sci. Rep. **8**, 1588 (2018).
18. Z. Gao, Z. Yang, F. Gao, H. Xue, Y. Yang, J. Dong, and B. Zhang, Phys. Rev. B **96**, 201402 (2017).
19. X. Wu, Y. Meng, J. Tian, Y. Huang, H. Xiang, D. Han, and W. Wen, Nat. Commun. **8**, 1304 (2017).
20. L. Ye, Y. Yang, Z. H. Hang, C. Qiu, and Z. Liu, Appl. Phys. Lett. **111**, 251107 (2017).
21. J. Noh, S. Huang, K. P. Chen, and M. C. Rechtsman, Phys. Rev. Lett. **120**, 063902 (2018).
22. Y. Kang, X. Ni, X. Cheng, A. B. Khanikaev, and A. Z. Genack, Nat. Commun. **9**, 3029 (2018).
23. F. Gao, H. Xue, Z. Yang, K. Lai, Y. Yu, X. Lin, Y. Chong, G. Shvets, and B. Zhang, Nat. Phys. **14**, 140 (2018).
24. B. Yan, Y. Peng, A. Shi, J. Xie, P. Peng, and J. Liu, Opt. Lett. **47**, 2044 (2022).
25. H. Xue, Y. Yang, and B. Zhang, Adv. Photonics Res. **2**, 2100013 (2021).
26. J. W. Liu, F. L. Shi, X. T. He, G. J. Tang, W. J. Chen, X. D. Chen, and J. W. Dong, Adv. Phys.: X **6**, 1905546 (2021).
27. M. Z. Hasan and C. L. Kane, Rev. Mod. Phys. **82**, 3045 (2010).
28. X. T. He, E. T. Liang, J. J. Yuan, H. Y. Qiu, X. D. Chen, F. L. Zhao, and J. W. Dong, Nat. Commun. **10**, 872 (2019).
29. M. I. Shalaev, W. Walasik, A. Xu, Y. Tsukernik, and N. M. Litchinitser, Nat. Nanotechnol. **14**, 31 (2019).
30. J. Ma, X. Xi, and X. Sun, Laser Photonics Rev. **13**, 1900087 (2019).
31. Y. Yang, Y. Yamagami, X. Yu, P. Pitchappa, J. Webber, B. Zhang, M. Fujita, T. Nagatsuma, and R. Singh, Nat. Photonics **14**, 446 (2020).
32. Y. Wu, X. Hu, and Q. Gong, Phys. Rev. Mater. **2**, 122201 (2018).
33. J. W. You, Q. Ma, Z. Lan, Q. Xiao, N. C. Panoiu, and T. J. Cui, Nat. Commun. **12**, 5468 (2021).
34. Y. Zeng, U. Chattopadhyay, B. Zhu, B. Qiang, J. Li, Y. Jin, L. Li, A. G. Davies, E. H. Linfield, B. Zhang, Y. Chong, and Q. J. Wang, Nature **578**, 246 (2020).
35. S. Barik, A. Karasahin, S. Mittal, E. Waks, and M. Hafezi, Phys. Rev. B **101**, 205303 (2020).
36. M. J. Mehrabad, A. P. Foster, R. Dost, E. Clarke, P. K. Patil, A. M. Fox, M. S. Skolnick, and L. R. Wilson, Optica **7**, 1690 (2020).
37. Z. Lan, J. W. You, Q. Ren, E. I. Wei, and N. C. Panoiu, Phys. Rev. A **103**, L041502 (2021).
38. X. Xie, S. Yan, J. Dang, J. Yang, S. Xiao, Y. Wang, S. Shi, L. Yang, D. Dai, Y. Yuan, N. Luo, T. Cui, G. Chi, Z. Zuo, B.-B. Li, C. Wang, and X. Xu, Phys. Rev. Appl. **16**, 014036 (2021).
39. H. Yoshimi, T. Yamaguchi, Y. Ota, Y. Arakawa, and S. Iwamoto, Opt. Lett. **45**, 2648 (2020).
40. C. W. Hsu, B. Zhen, S. L. Chua, S. G. Johnson, J. D. Joannopoulos, and M. Soljačić, Light: Sci. Appl. **2**, e84 (2013).
41. J. Chai, L. Liu, P. Hu, H. Xiang, and D. Han, Opt. Lett. **45**, 5652 (2020).
42. B. Zhen, C. W. Hsu, L. Lu, A. D. Stone, and M. Soljačić, Phys. Rev. Lett. **113**, 257401 (2014).
43. C. W. Hsu, B. Zhen, A. D. Stone, J. D. Joannopoulos, and M. Soljačić, Nat. Rev. Mater. **1**, 16048 (2016).
44. J. Jin, X. Yin, L. Ni, M. Soljačić, B. Zhen, and C. Peng, Nature **574**, 501 (2019).
45. X. Yin, J. Jin, M. Soljačić, C. Peng, and B. Zhen, Nature **580**, 467 (2020).
46. Y. Yang, C. Peng, Y. Liang, Z. Li, and S. Noda, Phys. Rev. Lett. **113**, 037401 (2014).
47. A. Cerjan, M. Jürgensen, W. A. Benalcazar, S. Mukherjee, and M. C. Rechtsman, Phys. Rev. Lett. **125**, 213901 (2020).
48. F. Yesilkoy, E. R. Arvelo, Y. Jahani, M. Liu, A. Tittl, V. Cevher, Y. Kivshar, and H. Altug, Nat. Photonics **13**, 390 (2019).
49. A. Kodigala, T. Lepetit, Q. Gu, B. Bahari, Y. Fainman, and B. Kanté, Nature **541**, 196 (2017).
50. Z. Zhang, Z. Lan, Y. Xie, M. L. N. Chen, W. E. I. Sha, and Y. Xu, Phys. Rev. Appl. **16**, 064036 (2021).
51. M. Born and E. Wolf, *Principle of Optics* (Cambridge University Press, 1999), 31.
52. M. L. N. Chen, L. J. Jiang, Z. Lan, and W. E. I. Sha, Opt. Express **28**, 14428 (2020).